Science Translational Medicine AAAS

Noninvasive Electroanatomic Mapping of Human Ventricular Arrhythmias with Electrocardiographic Imaging

Yong Wang, *et al.*

Sci Transl Med **3**, 98ra84 (2011);
DOI: 10.1126/scitranslmed.3002152

Editor's Summary

A New View of the Beating Heart

Just as a tree's shadow is an oversimplification of branches and foliage, the electrocardiogram, a decades-old tool for measuring the electrical activity of the heart, captures only an approximate view of the heartbeat, distorted by the intervening tissues between the heart and the few electrodes on the skin. This poses a problem when trying to treat heart diseases such as dangerous ventricular arrhythmias, which destabilize the heartbeat and can lead to sudden cardiac death. Now, with a technique called electrocardiographic imaging (ECGI), Wang and colleagues have married multiple electrical recordings from the skin of patients who have ventricular tachycardia (VT) with detailed computerized axial tomography (CAT) scans of the anatomy of their torso. From these data, the authors can back calculate what is happening, electrically speaking, on the surface of the misbehaving hearts, yielding an individual portrait of that patient's beating heart so that treatment can be more effectively deployed.

Twenty-five patients with VT were scheduled to undergo electrical mapping of their hearts and then ablation of heart tissue to correct the electrical defect with an invasive catheter. The authors augmented this standard treatment by creating an image of their beating hearts with noninvasive ECGI, before the standard procedure. The ECGI and standard procedure identified the same origination point of the tachycardia in almost all of the patients, and ECGI was able to correctly categorize both focal and reentrant mechanisms of VT. The time resolution of ECGI enabled the authors to follow the response of the heart to different patterns of stimulation (or pacing), revealing presystolic activation near the site of origin. They could see variable beat-to-beat conduction patterns and showed that the abnormal conduction patterns often began in regions of scar tissue, relics of previous heart attacks.

ECGI yields information comparable to the current procedure for mapping abnormal heart activity with a catheter-fed electrode, repeatedly placed on the heart surface. But it has significant advantages over the current approach: The spatial resolution of the ventricular arrhythmia on the heart surface is high, and it takes into account patient-to-patient variability in body size and shape. Further, it is noninvasive and can map single heartbeats, allowing unprecedented visualization of the anatomy of the electrical activation and beat-to-beat variability. These advantages should enable more effective diagnosis of VT and more appropriate drug or ablation therapy, which can now be directed to the specific characteristics of the patient's heart instead of a simplified shadow.

Science Translational Medicine (print ISSN 1946-6234; online ISSN 1946-6242) is published weekly, except the last week in December, by the American Association for the Advancement of Science, 1200 New York Avenue NW, Washington, DC 20005.

CARDIOVASCULAR DISEASE

Noninvasive Electroanatomic Mapping of Human Ventricular Arrhythmias with Electrocardiographic Imaging (ECGI)

Yong Wang,[1]* Phillip S. Cuculich,[1,2]* Junjie Zhang,[1] Kavit A. Desouza,[1] Ramya Vijayakumar,[1] Jane Chen,[1,2] Mitchell N. Faddis,[1,2] Bruce D. Lindsay,[3] Timothy W. Smith,[1,2] Yoram Rudy[1,2†]

The rapid heartbeat of ventricular tachycardia (VT) can lead to sudden cardiac death and is a major health issue worldwide. Efforts to identify patients at risk, determine mechanisms of VT, and effectively prevent and treat VT through a mechanism-based approach would all be facilitated by continuous, noninvasive imaging of the arrhythmia over the entire heart. Here, we present noninvasive real-time images of human ventricular arrhythmias using electrocardiographic imaging (ECGI). Our results reveal diverse activation patterns, mechanisms, and sites of initiation of human VT. The spatial resolution of ECGI is superior to that of the routinely used 12-lead electrocardiogram, which provides only global information, and ECGI has distinct advantages over the currently used method of mapping with invasive catheter-applied electrodes. The spatial resolution of this method and its ability to image electrical activation sequences over the entire ventricular surfaces in a single heartbeat allowed us to determine VT initiation sites and continuation pathways, as well as VT relationships to ventricular substrates, including anatomical scars and abnormal electrophysiological substrate. Thus, ECGI can map the VT activation sequence and identify the location and depth of VT origin in individual patients, allowing personalized treatment of patients with ventricular arrhythmias.

INTRODUCTION

Ventricular arrhythmias in the heart are a major cause of death and disability. In the past several decades, implantable and wearable defibrillator technologies have been developed to terminate ventricular tachycardia (VT), a life-threatening regular and repetitive fast heart rhythm, and ventricular fibrillation (VF), an irregular fast heart rhythm that is even more lethal (*1*–*3*). In addition, anti-arrhythmic drugs have been developed to prevent VT, but these have had limited success. Invasive procedures to modify the arrhythmic ventricular tissue to prevent VT have also been used, beginning with cardiac surgery to resect areas of scar (*4*–*6*). More recently, substrate modification has been achieved with radio-frequency ablation delivered at the tip of a steerable catheter inserted into the heart through a blood vessel (*7*–*10*). Nevertheless, invasive catheter mapping and ablation of the arrhythmic substrate is not a widely available procedure, and successful long-term outcomes from the procedure have been modest. Sudden death from ventricular arrhythmias remains a leading cause of death worldwide. Reasons for this include inability of current diagnostic tools to accurately identify patients at risk for sudden death, the limitations of invasive techniques for intracardiac mapping of cardiac electrical activation during arrhythmia, and incomplete knowledge about how and why VT and VF occur in a particular patient at a particular point in time.

Current routine noninvasive detection and diagnosis of the cardiac electrical activity is performed with a 12-lead electrocardiogram (ECG), a widely used test that is part of routine medical care. However, this century-old technology measures the reflection of cardiac electrical activity on the surface of the body, not on the heart itself. Therefore, it has limited spatial resolution for determining regional cardiac electrical activity and limited ability to locate regions of arrhythmic activity in the heart. These limitations are highlighted when the ECG is compared to currently available cardiac imaging tools, such as echocardiography, computed tomography (CT), and magnetic resonance imaging (MRI). A similar noninvasive method that provides high spatial resolution maps of abnormal electrical activity on the heart surface (rather than on the body surface) could contribute greatly to our understanding of the mechanisms of ventricular arrhythmias and to the diagnosis and treatment of cardiac rhythm disorders in patients. It could also help to identify patients at risk of sudden cardiac death and to develop mechanism-based therapy and guide patient-specific treatments. Here, we present such a noninvasive imaging method [electrocardiographic imaging (ECGI)] for electroanatomic mapping of cardiac electrical activation, as applied in a series of 25 patients undergoing catheter ablation procedures for various forms of VT.

RESULTS

ECGI (Fig. 1) combines body surface electrical potentials and heart-torso anatomical geometry to noninvasively determine the local electrical signals of the heart (electrograms) over the entire surface of both the left and the right ventricles (*11*–*13*). Using the relative timing of the constructed electrograms, activation sequences (isochrones) can be constructed in color-coded maps, and the propagation of activation wavefronts can be depicted in animated movies. ECGI images are constructed continuously and do not require the accumulation of data from multiple beats.

Twenty-five patients were referred for evaluation of symptomatic VT or premature ventricular contractions (PVCs). One patient underwent

[1]Cardiac Bioelectricity and Arrhythmia Center, Washington University, St. Louis, MO 63110, USA. [2]Cardiovascular Diseases, Department of Medicine, Washington University School of Medicine, St. Louis, MO 63110, USA. [3]Cardiovascular Medicine, Cleveland Clinic, Cleveland, OH 44195, USA.
*These authors contributed equally to this work.
†To whom correspondence should be addressed. E-mail: rudy@wustl.edu

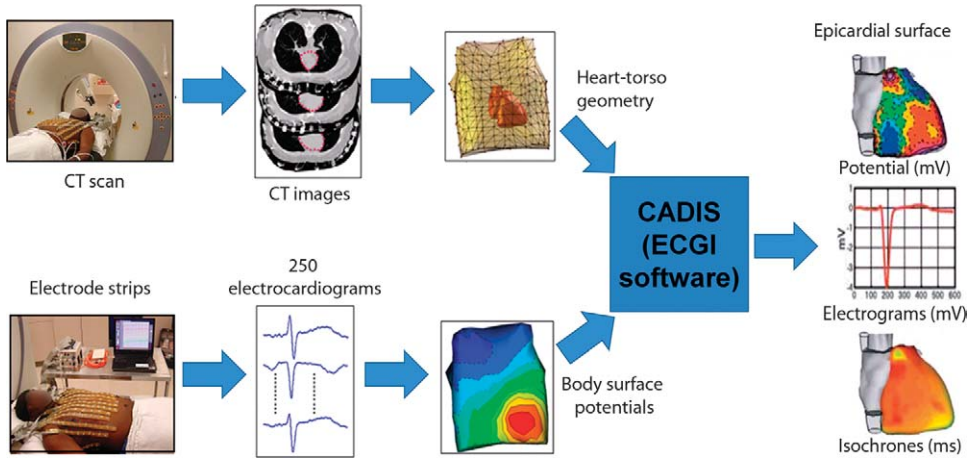

Fig. 1. ECGI methodology. Two hundred and fifty carbon electrodes mounted in strips are applied to the patient's torso before a pre-procedural thoracic CT scan, which provides cardiac geometry and torso-electrode positions in the same reference frame. The electrodes are connected to a multichannel mapping system. The electrical and anatomical data are processed mathematically to obtain noninvasive ECGI epicardial images that include potential maps, electrograms, isochronal activation sequences, and repolarization patterns. An ECGI movie of normal epicardial activation is provided in the Supplementary Material as reference (control) for the VT data (movie S1).

Table 1. Patient population. Patients are identified on the basis of VT localization: RVX for patient X with right ventricular localization, and LVX for patient X with left ventricular localization. PVC, premature ventricular complex; VT, ventricular tachycardia.

Patient number	Age, gender	Clinical presentation	Ejection fraction (%)	Ventricular substrate	Anti-arrhythmic medication
RV1	40, female	Sustained VT	60	Inferior nonischemic scar	β-Blocker
RV2	42, male	Nonsustained VT	70	No scar	β-Blocker
RV3	57, female	Sustained VT	65	No scar	β-Blocker
RV4	21, male	Nonsustained VT	58	No scar	β-Blocker
RV5	75, male	Sustained VT	35	Anterior ischemic scar	β-Blocker
RV6	51, female	Sustained VT	55	No scar	Amiodarone, β-blocker
RV7	46, female	Nonsustained VT	60	No scar	β-Blocker
RV8	37, female	Syncope, Nonsustained VT	55	No scar	Sotalol, β-blocker
RV9	57, male	High burden PVCs	40	Nonischemic cardiomyopathy	Sotalol, β-blocker
RV10	52, female	Symptomatic PVCs	50	Minimal scar, with previous ablation	β-Blocker
RV11	53, male	Symptomatic PVCs	60	No scar	None
LV1	63, female	Sustained VT	10	Nonischemic cardiomyopathy	Amiodarone, mexiletine, β-blocker
LV2	58, male	Sustained VT	40	Inferior ischemic scar	β-Blocker
LV3	45, male	Syncope, sustained VT	55	Lateral nonischemic scar (sarcoid)	β-Blocker, lidocaine
LV4	35, male	Sustained VT	70	No scar	Calcium channel blocker
LV5	52, female	Sustained VT	65	No scar	Amiodarone
LV6	46, male	Sustained VT	40	Anterolateral nonischemic scar (sarcoid)	Sotalol, mexiletine, β-blocker
LV7	48, female	Nonsustained VT	40	Nonischemic cardiomyopathy	β-Blocker
LV8	71, male	Sustained VT	40	Valvular cardiomyopathy	Sotalol
LV9	71, male	Sustained VT	25	Inferior ischemic scar	Amiodarone, lidocaine
LV10	42, male	Syncope, PVCs	45	Nonischemic (Kawasaki disease)	β-Blocker
LV11	71, male	Sustained VT	25	Anterior ischemic scar	Amiodarone
LV12	81, male	Syncope, sustained VT	30	Anterior, inferior, and lateral ischemic scar	Amiodarone, β-blocker
LV13	62, male	Sustained VT	30	Nonischemic cardiomyopathy	Amiodarone, mexiletine, β-blocker
LV14	67, male	Sustained VT	25	Apical ischemic scar	Amiodarone, mexiletine, β-blocker
LV15	54, male	Nonsustained VT	45	No scar	Lidocaine, β-blocker

two different studies several months apart, for a total of 26 ECGIs performed. This group of patients participated in a total of 23 catheter-based electrophysiology studies (EPSs) in which we planned to initiate the ventricular arrhythmia, map its origin and circuit (if possible), and ablate the necessary tissue to render the arrhythmia noninducible. We performed noninvasive ECGI before the invasive EPS in those patients who demonstrated spontaneous abnormal ventricular rhythms (18 patients, 19 studies). ECGI was performed during the EPS in other patients (four patients). Nine patients were imaged during sustained VT; the remaining patients were imaged during PVCs.

Patients were identified on the basis of their VT localization: RVX for patient X with right ventricular (RV) localization, and LVX for patient X with left ventricular (LV) localization. Pertinent medical records are summarized in Table 1. The mean age for the cohort was 54 years (range, 21 to 81 years). Results of the corresponding EPS, including 12-lead ECG morphology, cycle length, and information regarding induction, testing, and ablation of the tachycardia, are detailed in the Supplementary Material (compiled in table S2).

We used ECGI to characterize each tachycardia on the basis of analysis of the isochrone (color-coded map depicting the location of the activation wavefront over time), potential, local electrogram, and wavefront propagation information. A three-step process, created from previously validated findings (*11*–*13*), was used for each patient: (i) localize the site of origin (SOO) of the arrhythmia from isochrone and potential maps; (ii)

Table 2. Comparison of noninvasive ECGI with invasive EP study. Patients are identified on the basis of VT localization: RVX for patient X with right ventricular localization, and LVX for patient X with left ventricular localization. Discrepancies between ECGI and EPS are in bold. Because of the thin tissue in the outflow tract, patients with outflow tract SOO were excluded from myocardial depth analysis. Arrhythmias starting from a focal origin and spreading radially in the ECGI activation map are classified as "radial," because ECGI cannot differentiate between focal mechanism and microreentry. LV, left ventricle; RV, right ventricle; RVOT, right ventricular outflow tract; N/A, not available.

Patient number	Localization		Mechanism		Myocardial depth	
	ECGI	EPS	ECGI	EPS	ECGI	EPS
			Right ventricle			
RV1	Anterior-left RVOT	Anterior-left RVOT	Radial	Focal	Excluded	Excluded
RV2	Mid-septal RVOT	Mid-septal RVOT	Radial	Focal	Excluded	Excluded
RV3	Mid-septal RVOT	Mid-septal RVOT	Radial	Focal	Excluded	Excluded
RV4	Posterior-right RVOT	Posterior-right RVOT	Radial	Focal	Excluded	Excluded
RV5	Anterior-left RVOT	N/A	Radial	N/A	Excluded	Excluded
RV6	Free wall RVOT	Free wall RVOT	Radial	Focal	Excluded	Excluded
RV7	Mid-septal RVOT	Mid-septal RVOT	Radial	Focal	Excluded	Excluded
RV8	Free wall RVOT	Free wall RVOT	Radial	Focal	Excluded	Excluded
RV9	Mid-septal RVOT	Mid-septal RVOT	Radial	Focal	Excluded	Excluded
RV10	**Inferior basal lateral RV**	**Inferior basal septal RV**	Radial	Focal	Epicardial	Epicardial
RV11	Posterior-right RVOT	Posterior-right RVOT	Radial	Focal	Excluded	Excluded
			Left ventricle			
LV1	Lateral apical LV	Lateral apical LV	Radial	Focal	Epicardial	Epicardial
LV2	Inferior basal septal LV	Inferior basal septal LV	Reentry	Reentry	Fractionated	Endocardial
LV3	Inferior lateral apical LV	Inferior lateral apical LV	Reentry	Reentry	Fractionated	Mid-myocardial
LV4	Apical septal LV	Fascicular	Radial	Focal	Intramural	Endocardial
LV5	Apical septal LV	Fascicular	Radial	Focal	Intramural	Endocardial
LV6	Anterior basal LV	Anterior basal LV	Radial	Focal	Epicardial	Epicardial
LV7	Left coronary cusp	Left coronary cusp	Radial	Focal	Excluded	Excluded
LV8	Lateral basal LV	N/A	Reentry	N/A	Epicardial	N/A
LV9	Septal basal LV	Septal basal LV	Reentry	Reentry	Fractionated	Endocardial
LV10	Septal basal LV	N/A	Radial	N/A	Epicardial	N/A
LV11	**Anterior LV**	**Apical LV**	Reentry	Reentry	Fractionated	Mid-myocardial
LV12	Inferior basal LV	N/A	Reentry	N/A	Fractionated	N/A
LV13	Lateral basal LV	Lateral basal LV	Radial	Focal	Epicardial	Epicardial
LV14	Mid-anterior LV	Mid-anterior LV	Reentry	Reentry	Fractionated	Endocardial
LV15	LV summit	Great cardiac vein	Radial	Focal	Epicardial	Epicardial

evaluate the mechanism by observing the three-dimensional propagation pattern and its relationship to the myocardial substrate; and (iii) approximate the myocardial depth of the origin with local electrograms (pure Q wave for epicardial origin, rS complex for intramural or endocardial origin). Representative examples of specific instances of cardiac physiology are shown in the text. Detailed maps of ventricular arrhythmias for all ECGI studies are shown in the Supplementary Material, comprising a collection of noninvasively mapped human VTs (figs. S2 to S27). Movies of electrical activation are provided for a subset of representative cases (movies S2 to S13). The Supplementary Material also includes a map and movie of a normal ventricular activation pattern for reference (fig. S1 and movie S1).

Location of VT initiation

On the basis of the invasive EPS, 11 patients had an SOO in the RV, including 9 patients in which the SOO was in the RV outflow tract. Twelve patients had an SOO in the LV. When we compared the results from ECGI to those from invasive EPS (Table 2), ECGI correctly identified the LV or RV SOO 100% of the time (23 of 23). When we compared the specific locations within each ventricle, noninvasive ECGI SOO was in agreement with invasive EPS SOO in 10 of 11 RV sites (91%) and in 11 of 12 LV sites (92%). Examples of ECGI localization can be found in Fig. 2.

For the two patients with discrepancies between invasive EPS and noninvasive ECGI (patients RV10 and LV11), the discrepant locations were in proximity to each other. For patient RV10, ECGI imaged the right posterolateral base as the SOO, whereas EPS suggested the right posteroseptal base as the SOO. This patient had undergone previous ablations of a right posteroseptal accessory pathway and a right atriofascicular pathway in the posterolateral base. We suspect that the previous ablations in these locations may have played a role in the differences between ECGI and EPS. For patient LV11, ECGI imaged the mid-anterior LV as the SOO, whereas EPS suggested a more apical LV location as the SOO. This patient had a large LV apical aneurysm and had several different VT morphologies. It is possible that ECGI and EPS imaged two different VTs.

Mechanisms of VT

During the invasive EPS, the arrhythmia mechanism can be characterized on the basis of the heart's response to ventricular pacing at a faster rate than the tachycardia and resetting of the VT, a process known as entrainment. On the basis of invasive EPS, 18 patients were found to have focal VT (activation starting from a focal site and inability to reproducibly entrain the tachycardia with ventricular pacing), whereas 5 patients had a reentrant mechanism (activation forming a rotational wave comprising nearly all of the tachycardia cycle length and successful entrainment of the tachycardia with stable return cycle lengths after cessation of pacing). For the patients with focal VTs, noninvasive ECGI activation maps uniformly showed a radial activation pattern from the SOO (18 of 18). In all the patients with a reentrant mechanism, noninvasive ECGI showed a rotational wavefront with a high degree of curvature (five of five), with the wavefront returning to the initiation site. Examples of these two distinct propagation patterns are shown in Fig. 3. Detailed descriptions and selected movies of activation are in the Supplementary Material. It should be emphasized that the five reentrant VTs imaged by ECGI involved a macro-reentry circuit (a long, looping path of continuous electrical activation). It is not known whether ECGI can differentiate mechanistically between micro-reentry and focal activation.

The use of ECGI during induction of VT by programmed stimulation in the EP lab allowed us to visualize arrhythmogenesis in a closed-chest human heart. An example is Fig. 4, in which programmed ventricular stimulation initiated sustained VT. Figure 4A shows baseline pacing (cycle length = 600 ms) from a catheter placed in the RV apex, marked with +. A line of conduction block through which the wavefront cannot directly pass is seen in the lateral LV (thick black line). Figure 4B shows premature pacing (S1 – S2 = 280 ms) from the same location, which resulted in functional extension of the line of block. Figure 4C demonstrates the first beat of induced VT, marked with *, which originated from the last area that was activated by the premature paced beat in Fig. 4B, suggesting triggered activity as the mechanism (*14*). The delayed activation of this region by premature pacing promotes recovery and capture of adjacent myocardium by the first

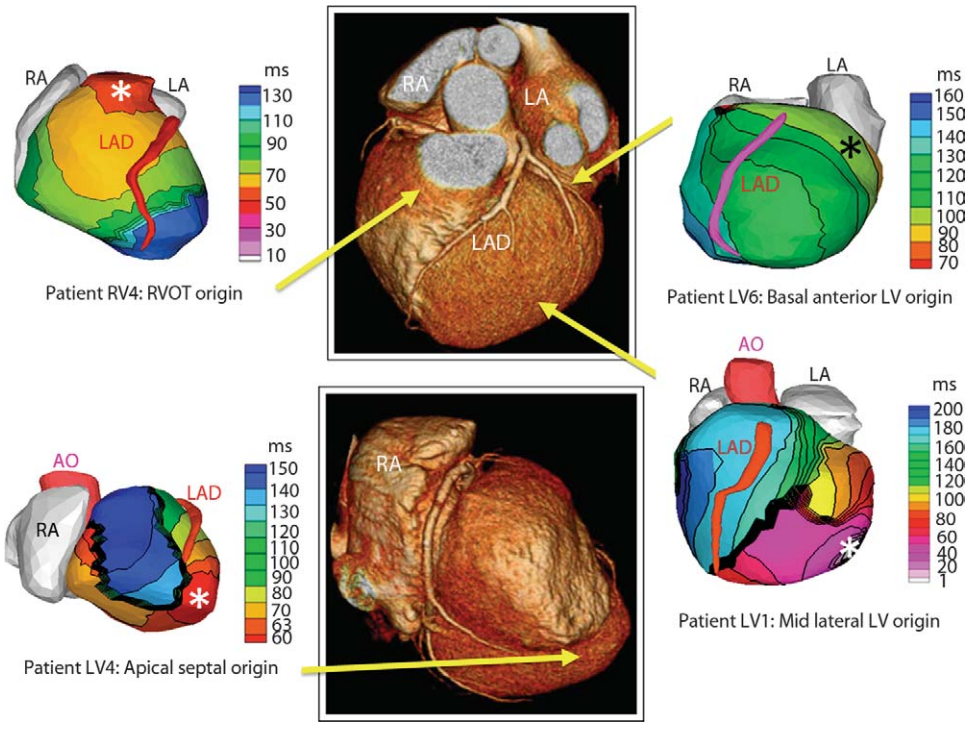

Fig. 2. Examples of noninvasive ECGI isochrone maps for localization of VT site of origin. Epicardial isochrone maps are shown for four patients, with earliest epicardial activation marked with an asterisk (see Supplementary Material for detailed description of activation sequences). EP study–determined sites of origin are indicated under the ECGI maps. Yellow arrows point to VT origin on a representative CT scan. RA, right atrium; LA, left atrium; AO, aorta; LAD, left anterior descending coronary artery; LV, left ventricle; RVOT, right ventricular outflow tract.

beat of VT excitation. In this case, during the invasive EPS, the VT had variable responses to pacing entrainment maneuvers, which is more characteristic of focal triggered activity than reentrant mechanism.

In addition to VT initiation, ECGI provided images of VT maintenance. As shown in the activation movies S5 and S6, local presystolic activation was often imaged 5 to 10 ms before the subsequent beats of both reentry and focal VT. The presystolic activation was always near the SOO of the VT and was often consistent from beat to beat. This finding was apparent on ECGI of patients with VT of both epicardial origin (1:02 and 1:13 in movie S5) and endocardial origin (0:14, 0:27, and 0:50 in movie S6).

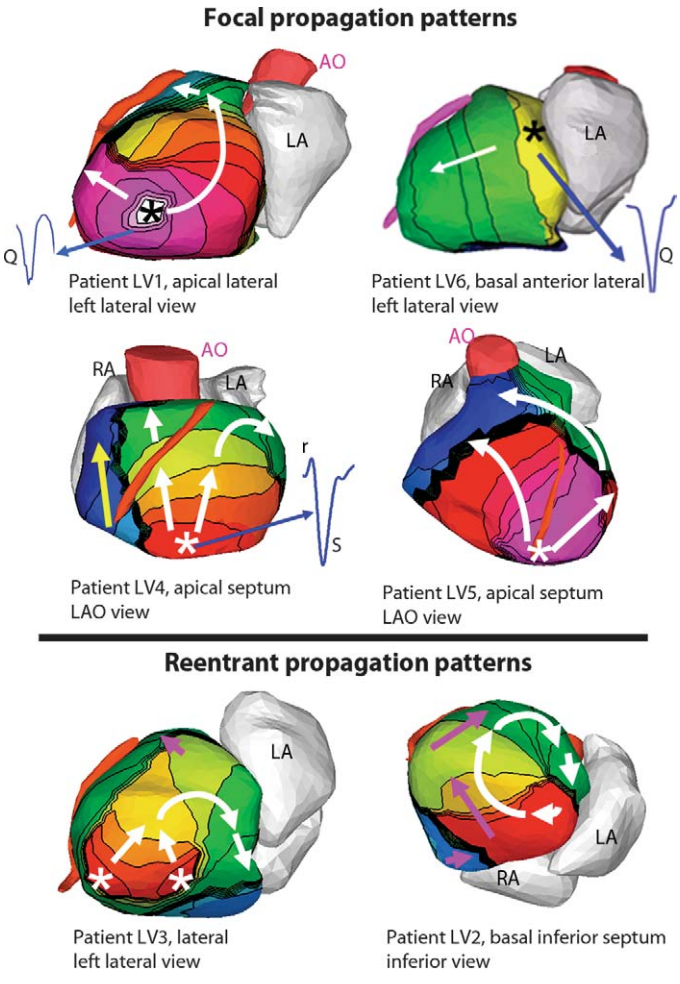

Fig. 3. ECGI imaged propagation patterns, origins, and local electrograms for VT. Isochrone maps for six patients, with earliest epicardial activation marked with an asterisk (see Supplementary Material for detailed descriptions of activation sequences). (Top) Focal propagation patterns. Tachycardias that were determined to be focal during EP studies demonstrate a radial spread (white arrows) away from the early activation point (asterisk). Yellow arrows indicate later phases of ventricular activation. (Bottom) Reentrant propagation patterns. Tachycardias that were determined to be reentrant during EP studies show a rotational activation pattern (white arrows). Thick black lines indicate conduction block. Purple arrows indicate later phases of ventricular activation. (Insets) Several epicardial electrograms from sites of earliest activation are shown in blue, highlighting the presence or absence of *r* wave. Pure Q morphology indicates epicardial origin; rS morphology indicates intramural origin. Description under each image indicates the location of VT initiation and identifies the displayed view of the heart. LAO, left anterior oblique.

For all five patients with reentrant VT, the VT activation pattern was related to areas of ventricular scar, as shown in the example of Fig. 5. Figure 5B shows ECGI during VT, where the earliest activation is in the inferior basal septum (red). The wavefront initially exits this area at the start of the VT beat and completes the beat by reentering this area (arrows). Local presystolic activation was imaged at the scar border immediately before each VT beat, indicating exit sites of slowly propagating wavefronts through the scar (see movie S6). Figure 5C (left) shows results from the clinical nuclear myocardial perfusion images [single-photon emission computed tomography (SPECT)]. For this study, technetium-99m was administered intravenously and was incorporated into living cardiac myocytes. Imaging the absence of this isotope in regions of the heart allowed identification of scar tissue, most often a result of a myocardial infarction. In Fig. 5C (left), the area of the scar from a previous infarction is located in the inferior septum (dark blue). Invasive catheter mapping (Fig. 5C, right) during tachycardia confirmed the origin of VT in the inferior septum. Pacing entrainment maneuvers confirmed a reentrant mechanism, and radio-frequency ablation, applied through the tip of a catheter in this region (red marks), terminated the tachycardia.

Although monomorphic VT is thought to arise from a single location, localized beat-to-beat changes in the ventricular activation pattern can be seen with ECGI. This may be a result of different exit points from a ventricular scar (Fig. 6) or functional changes related to ventricular excitation and recovery properties, as shown in movie S9. Figure 6 shows ECGI during a monomorphic VT from an infiltrative cardiomyopathy in the lateral LV. Figure 6A shows activation patterns for three consecutive VT beats (T1, T2, and T3) in three views. ECGI identified two distinct areas of early epicardial activation (white asterisks), which differed slightly from beat to beat. The propagation pattern varied depending on the relative contribution of the two sources, but for all beats, the wavefront turned clockwise and propagated toward the LV lateral base with a high degree of curvature, where it reached a line of block in the inferolateral base. ECGI movies of this phenomenon are available online (movie S7). Figure 6B shows a gadolinium-enhanced MRI image, which revealed a patch of myocardial enhancement in the lateral LV (white arrows), consistent with a focal myocarditis or cardiac sarcoid. Figure 6C shows the invasive electroanatomic map created during the presenting VT (Tx). The region of earliest activation is white (black arrows). Figure 6D shows the invasive electroanatomic map created during a different VT (Ty) after initial ablation at the site of earliest activation. The earliest activation site (black arrows) is shifted more apically. Twelve-lead surface ECGs of the two VT morphologies (Tx and Ty) are shown. In this example, noninvasive ECGI was able to accurately identify the spontaneous, dynamic, beat-to-beat transitions of VT activation patterns, which were not easily recognized on the 12-lead ECG. Examples of similar beat-to-beat changes during VT, imaged by ECGI, can be found in the Supplementary Material (figs. S17, S21, and S25 and movies S9 and S12).

Myocardial depth

Invasive EPS findings were compared with ECGI for determining epicardial or intramural locations of VT. Because of the thin tissue in the outflow tract, patients with outflow tract SOO were excluded. Of the

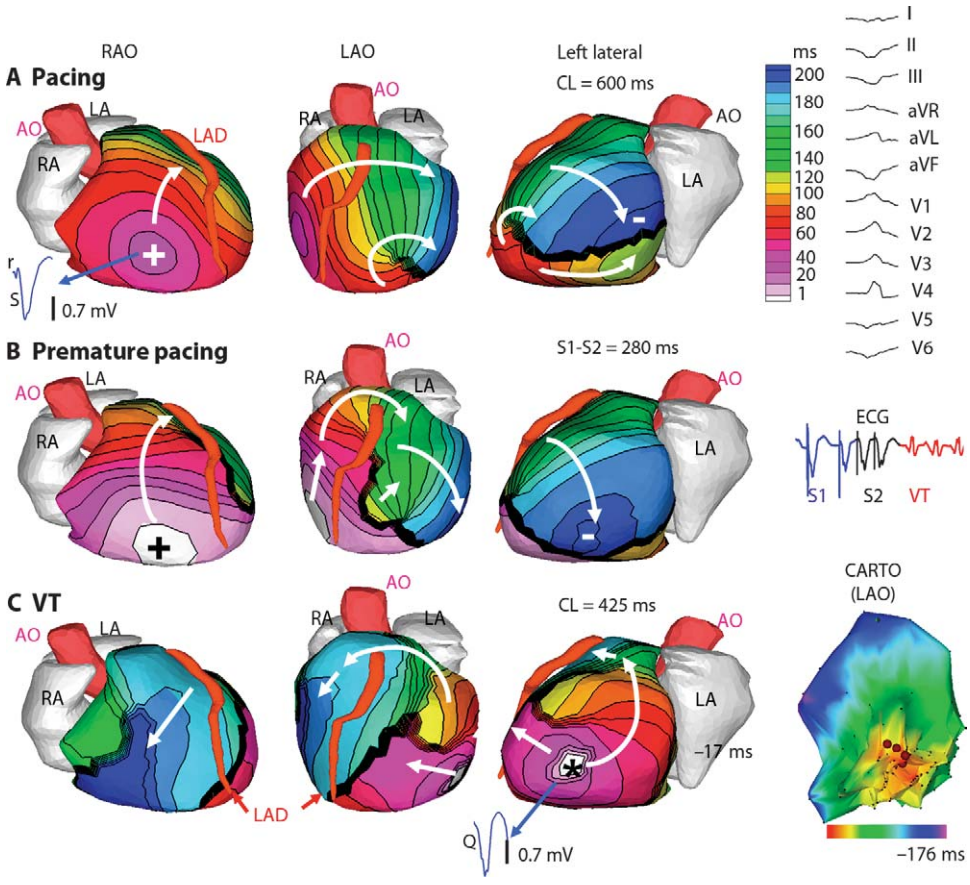

Fig. 4. Example ECGI of focal VT induced by programmed electrical stimulation (patient LV1). (**A**) Epicardial activation sequence during drive train (S1) pacing at a cycle length (CL) of 600 ms. RAO, right anterior oblique. White arrows show direction of wavefront propagation. Thick black line indicates conduction block. Earliest epicardial activation site is marked by + and corresponds to the underlying endocardial pacing site. ECGI epicardial electrogram from this site is shown at the left (blue), with rS complex consistent with endocardial activation. (Right) Twelve-lead surface ECG during VT. (**B**) Premature (S2) pacing at 280-ms coupling interval from the same pacing site. The major wavefront is forced to pivot around the extended line of conduction block. There is some fusion with an intramural transseptal front (small white arrow). (Right) Recording from a single-lead ECG. All S1 beats (blue) are similar, as are the two S2 beats (black) and all the VT beats (red). (**C**) VT. The earliest epicardial activation site is marked by an asterisk. ECGI electrogram from the VT origin site is shown (blue), with a pure Q wave, indicative of epicardial origin. (Right) Invasive LV endocardial activation map (CARTO) of the VT in the left anterior oblique projection (red is early). ECGI epicardial activation movies are in the Supplementary Material (movie S5).

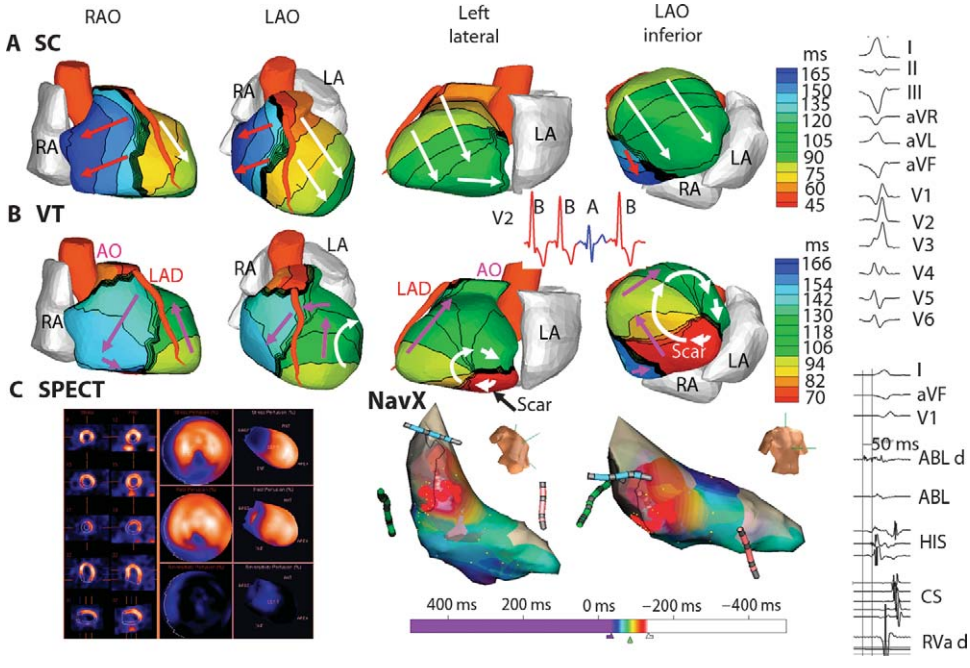

Fig. 5. Example ECGI of reentrant VT from inferobasal scar (patient LV2). (**A**) Four views of activation sequence during a sinus capture (SC) beat (blue on the V2 ECG). Arrows indicate direction of the activation wavefronts. (**B**) Activation sequence during VT beats (red on the V2 ECG). White arrows indicate a clockwise lateral loop (left lateral and left anterior oblique inferior views); purple arrows show propagation into the RV in a counterclockwise fashion. (**C**) (Left) SPECT images showing a scar at the inferobasal LV region (blue). (Right) Limited invasive endocardial map of VT activation (red, early; blue, late). ECGI epicardial activation movies, including early activation of a region near the inferior scar border, are in the Supplementary Material (movie S6). (Right column) (Top) Twelve-lead surface ECG during VT. (Lower) Ablation catheter signals. The earliest electrogram signal is seen at the inferoseptal border zone, 50 ms before the onset of the surface QRS. ABL d, bipolar electrogram at the distal ablation catheter; HIS, AV junction/His bundle; CS, coronary sinus; RVa d, right ventricular apex.

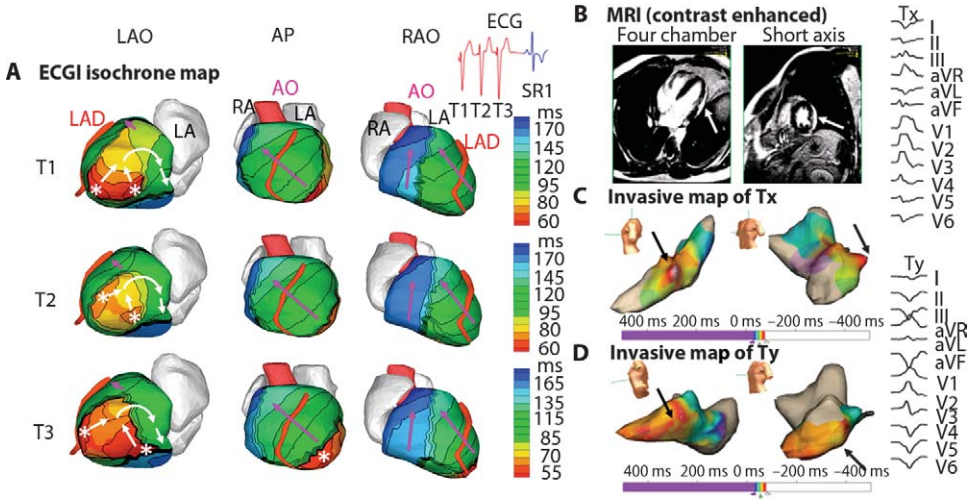

Fig. 6. Example of ECGI of reentrant VT in lateral wall infiltrative cardiomyopathy (patient LV3). (**A**) ECGI isochrone map. Activation patterns for three consecutive VT beats (T1, T2, and T3). ECGI identified two distinct areas of early epicardial activation (white asterisks), which differed from beat to beat. The propagation pattern varied somewhat depending on the relative contribution of the two sources, but for all beats, the wavefront turned clockwise and propagated to the LV lateral base with a high degree of curvature, where it reached a line of block in the inferolateral base. The corresponding movie is available in the Supplementary Material. (**B**) A gadolinium-enhanced MRI revealed a patch of myocardial enhancement in the lateral LV (white arrows), consistent with a focal myocarditis or cardiac sarcoid. (**C**) Invasive electroanatomic map created during the presenting VT (arbitrarily named Tx). The region of earliest activation is shown by black arrows. (**D**) Invasive electroanatomic map created during a different VT (arbitrarily named Ty) after initial ablation at the site of earliest activation. The earliest activation (black arrows) is shifted more apically. (Right) Twelve-lead surface ECGs of two VT morphologies (Tx and Ty). AP, anterior-posterior view; SR1, first sinus rhythm beat after VT.

13 remaining patients, the invasive EPS determined the SOO to be endocardial in 6, epicardial in 5, and mid-myocardial in 2. All five patients with epicardial SOO had a pure Q wave on the noninvasive ECGI electrogram at the site of earliest activation (100%), indicative of epicardial origin (*15*). Of the patients with a nonepicardial SOO, the local noninvasive ECGI electrogram at the earliest site demonstrated a small r wave in seven of eight (88%), indicative of an intramural initiation site (*15*).

DISCUSSION

This paper reports the use of a noninvasive, three-dimensional electroanatomic mapping system, ECGI, in a series of patients undergoing catheter ablation for a broad range of VTs. Our findings reveal a large diversity of human VT with respect to activation patterns, mechanisms, and sites of initiation (shown individually, including movies of dynamic progression, in the Supplementary Material). Over a wide range of VT locations and mechanisms, the noninvasive ECGI results were consistent with those of invasive catheter mapping.

In the clinical setting, ECGI has several advantages. It overcomes the main limitation of the standard body surface 12-lead ECG by providing high spatial resolution maps of ventricular arrhythmias on the heart surface. Where the 12-lead ECG requires interpretation of body surface data in terms of cardiac activity, assuming a "standard" heart shape and size in a "standard" torso, ECGI uses the patient's specific heart-torso geometry to identify the location of the arrhythmia and map its sequence on the heart. Additionally, ECGI offers distinct advantages over invasive catheter mapping, a technique in which the tip of a catheter is maneuvered inside the heart to hundreds of locations, and information about the continuing arrhythmia is gathered sequentially from each site. ECGI's advantages include its noninvasive nature and the ability to map the entire tachycardia in a single beat. The spatial resolution and ability to image continuously and simultaneously the activation sequences over the entire ventricular surfaces allowed us to make observations beyond the ability of current tools regarding VT initiation and continuation (Fig. 4) and regarding the relationship of the VT activation wavefront to the ventricular substrate (Figs. 5 and 6), including anatomical scars and abnormal electrophysiological substrate (lines of block, slow conduction). With the single beat, continuous mapping that ECGI provides, we were able to detect beat-to-beat dynamic changes in the origin and sequence of VT (Fig. 6).

The results suggest that ECGI can play a clinically useful role. From a treatment perspective, potential clinical advantages include the ability to assist in guiding the choice of medication on the basis of VT mechanism or pointing to the most effective strategy for catheter ablation. An example illustrates the potential benefit. Currently, when a patient has recurrent VT, especially when it is refractory to anti-arrhythmic medications, an EP mapping study with ablation is offered. An endocardial approach in which an electrode is inserted through veins to map the electrical activity of the heart is almost exclusively used as a first procedure; then, the operator tries to induce the arrhythmia with pacing and intravenous medications. The VT can be mapped accurately only if it is sustained over time. Mapping is a meticulous process in which electrical information is collected from the tip of a roving catheter on a point-by-point basis and that lasts for several hours. Ideally, for obtaining a detailed map of the arrhythmia, the mapping is performed during sustained VT. However, most patients in sustained VT have life-threatening low blood pressure, which does not allow the time for detailed mapping. Additionally, sustained VT can have deleterious cardiovascular effects. If at the end of mapping, or after unsuccessful endocardial ablation (performed by heating the tip of the catheter to eliminate electrical conduction of the diseased tissue), the operator deems the VT to be epicardial in origin, the procedure is halted, and a separate procedure to target the epicardium is scheduled at a later date. In contrast, if ECGI is used, the location and depth of the VT SOO can be determined in a single beat of arrhythmia, either during or before the procedure. The treating physician could then direct the catheter-based ablation procedure toward that area in a more focused and time-efficient manner. It is probable that the alternative ECGI-directed treatment would yield improved patient safety and beneficial

treatment outcomes, although this will require evaluation in a randomized clinical trial in a large population of VT patients.

The results presented here provide the basis for noninvasive arrhythmia diagnosis. Technologies such as high-frequency ultrasound (*16*, *17*) and gamma knife radiosurgery (*18*) are being developed for noninvasive ablation of cardiac tissue, paving the way for completely noninvasive diagnosis and treatment of VTs. The noninvasive nature of ECGI would also allow its use in testing the outcomes of treatment (by ablation or drugs) and examining heart activity changes over time.

There are several limitations to the clinical applicability of ECGI at this time. ECGI is still a research tool, and its limited availability precludes large-scale multicenter clinical studies at present. Further technical developments are needed to facilitate rapid application of the many body surface electrodes in the clinical setting, to automate the data analysis and map generation and display, and to build a user-friendly interface for the clinical operator. The body surface electrodes, placed with high density on the torso surface, often compete for skin area needed to place other clinical monitoring systems during the EP study. Finally, previous ECGI validation studies show accuracy of 4 to 6 mm in determining activation initiation sites. Future algorithm developments may allow for more precise mapping.

The most significant weakness to the current study involves the variable contributions of the endocardium and epicardium to the tachycardia circuits (*19*–*22*). As demonstrated in open chest mapping, the earliest epicardial activation of VT may not accurately identify the location of an endocardial circuit, although our data show close correlation between invasive endocardial mapping and noninvasive ECGI epicardial imaging. Additionally, because the ECGI-imaged activation sequence uses only the QRS complex for analysis, it does not image continuously during one cycle of tachycardia, known as cycle length. Slow, discontinuous diastolic conduction inside the scar (reflected in early activation detected by ECGI at the scar border zone; see example in movie S6) and intramural activation (ECGI is limited to the epicardium) likely continue during the time that ECGI does not image. Finally, analysis of the ECGI data collected in the EP lab (4 of the 26 cases) was subject to the bias of the investigator knowing the outcome of the EPS.

MATERIALS AND METHODS

All protocols were approved by the Institutional Review Board at Washington University in St. Louis, and informed consent was obtained from all patients. ECGI methodology was described previously (*11*–*13*). ECGI has been validated extensively under different physiological and pathological conditions in animal models (*13*, *15*, *23*–*26*) and in human studies (*11*, *12*, *27*–*42*). Two hundred and fifty-six carbon electrodes on strips were applied to the patient's torso. Small radio-opaque markers were attached to each electrode. All strips were connected to a portable mapping system (BioSemi). After electrode application, patients underwent thoracic non–contrast-gated CT scan with axial resolution of 3 mm. Scans were gated at 70% of the R-R interval (ventricular diastole) if patients were in sinus rhythm. For patients who underwent continued ECGI mapping during a subsequent EP study, the 256 carbon electrodes were kept in the same position. Patient-specific ventricular epicardial surface geometry and body surface electrode positions were labeled and digitized from CT images.

The 256 channels of body surface potentials were sampled at 1-ms intervals, and the data were saved on a laptop computer. Body surface potentials were acquired during sinus rhythm, VT, and programmed electrical stimulation, when available.

The body surface potential and geometrical information (torso-heart geometrical relationship) were combined by ECGI algorithms to noninvasively construct epicardial electrograms, activation sequences (isochrones), potential maps, and repolarization patterns (*11*, *12*). ECGI was constructed on a beat-by-beat basis and did not require accumulating data from many identical beats. Activation times were determined by the maximal negative slope of the epicardial electrograms. Activation movies for several consecutive beats were constructed by animating the activation wavefront on the patient-specific CT-derived epicardial surface. On the basis of the isochrone map, lines or regions of block (thick black lines in the map) were inferred if activation times in adjacent areas differed by more than 50 ms. Slow conduction is represented by crowded isochrones. The earliest site of epicardial activation was determined from the isochrone map and from the earliest potential minimum in the epicardial potential map (*13*).

The results of ECGI were processed independently from the results of the EP study. Additionally, EP operators did not have access to ECGI results before the procedure. Clinical cardiac testing results, such as invasive three-dimensional electroanatomic maps, gadolinium-enhanced cardiac MRI, and SPECT, were obtained retrospectively for each patient.

SUPPLEMENTARY MATERIAL

www.sciencetranslationalmedicine.org/cgi/content/full/3/98/98ra84/DC1
The complete data set of ECGI-imaged human ventricular tachycardia.
Fig. S1. Normal ventricular epicardial activation (see movie S1).
Fig. S2. Patient RV1: ECGI of an anterior-left RVOT tachycardia.
Fig. S3. Patient RV2: ECGI of a mid-septal RVOT tachycardia.
Fig. S4. Patient RV3: ECGI of a mid-septal RVOT tachycardia.
Fig. S5. Patient RV4: ECGI of a posterior-right RVOT tachycardia.
Fig. S6. Patient RV5: ECGI of an anterior-left RVOT tachycardia (noninducible during EPS).
Fig. S7. Patient RV6: ECGI of a free wall RVOT tachycardia.
Fig. S8. Patient RV7: ECGI of a mid-septal RVOT tachycardia (see movie S2).
Fig. S9. Patient RV8: ECGI of a free wall RVOT tachycardia.
Fig. S10. Patient RV9: ECGI of a mid-septal RVOT tachycardia (see movie S3).
Fig. S11. Patient RV10: ECGI of an RV base tachycardia.
Fig. S12. Patient RV11: ECGI of a posterior-right RVOT tachycardia (see movie S4).
Fig. S13. Patient LV1: ECGI of a focal ventricular tachycardia induced by programmed electrical stimulation (with movie S5).
Fig. S14. Patient LV2: ECGI of reentrant VT from inferobasal scar (with movie S6).
Fig. S15. Patient LV3: ECGI of a reentrant VT from mid-lateral LV (lateral wall infiltrative cardiomyopathy) (with movie S7).
Fig. S16. Patient LV4: ECGI of left posterior fascicular VT (with movie S8).
Fig. S17. Patient LV5: ECGI of a left fascicular VT (with movie S9).
Fig. S18. Patient LV6: ECGI of an epicardial anterior basal focal VT.
Fig. S19. Patient LV7: ECGI of tachycardia originating in the left coronary cusp of the aorta.
Fig. S20. Patient LV8: ECGI of a basal mitral annular PVC.
Fig. S21. Patient LV9: ECGI of an inferior septal VT.
Fig. S22. Patient LV10: ECGI of an inferior lateral mitral annular PVC.
Fig. S23. Patient LV11: ECGI of apical scar–related reentrant VT (with movie S10).
Fig. S24. Patient LV12: ECGI of an inferior basal LV PVC (with movie S11).
Fig. S25. Patient LV13: ECGI of pleomorphic PVCs from the posterolateral LV (with movie S12).
Fig. S26. Patient LV14: ECGI of a VT from the anterior-apical LV in a patient with an apical aneurysm (with movie S13).
Fig. S27. Patient LV15: ECGI of a VT from the anterior interventricular vein/distal coronary sinus.
Table S1. Results from EP studies.
Movie S1. Normal: Normal ventricular activation pattern.
Movie S2. Patient RV7 activation pattern.

Movie S3. Patient RV9 activation pattern.
Movie S4. Patient RV11 activation pattern.
Movie S5. Patient LV1 activation pattern.
Movie S6. Patient LV2 activation pattern.
Movie S7. Patient LV3 activation pattern.
Movie S8. Patient LV4 activation pattern.
Movie S9. Patient LV5 activation pattern.
Movie S10. Patient LV11 activation pattern.
Movie S11. Patient LV12 activation pattern.
Movie S12. Patient LV13 activation pattern.
Movie S13. Patient LV14 activation pattern.

REFERENCES AND NOTES

1. A. J. Moss, W. J. Hall, D. S. Cannom, J. P. Daubert, S. L. Higgins, H. Klein, J. H. Levine, S. Saksena, A. L. Waldo, D. Wilber, M. W. Brown, M. Heo, Improved survival with an implanted defibrillator in patients with coronary disease at high risk for ventricular arrhythmia. Multicenter Automatic Defibrillator Implantation Trial Investigators. *N. Engl. J. Med.* **335**, 1933–1940 (1996).
2. A comparison of antiarrhythmic-drug therapy with implantable defibrillators in patients resuscitated from near-fatal ventricular arrhythmias. The Antiarrhythmics versus Implantable Defibrillators (AVID) Investigators. *N. Engl. J. Med.* **337**, 1576–1583 (1997).
3. A. E. Buxton, K. L. Lee, J. D. Fisher, M. E. Josephson, E. N. Prystowsky, G. Hafley, A randomized study of the prevention of sudden death in patients with coronary artery disease. Multicenter Unsustained Tachycardia Trial Investigators. *N. Engl. J. Med.* **341**, 1882–1890 (1999).
4. J. H. Wittig, J. P. Boineau, Surgical treatment of ventricular arrhythmias using epicardial, transmural, and endocardial mapping. *Ann. Thorac. Surg.* **20**, 117–126 (1975).
5. G. Guiraudon, G. Fontaine, R. Frank, G. Escande, P. Etievent, C. Cabrol, Encircling endocardial ventriculotomy: A new surgical treatment for life-threatening ventricular tachycardias resistant to medical treatment following myocardial infarction. *Ann. Thorac. Surg.* **26**, 438–444 (1978).
6. L. N. Horowitz, A. H. Harken, J. A. Kastor, M. E. Josephson, Ventricular resection guided by epicardial and endocardial mapping for treatment of recurrent ventricular tachycardia. *N. Engl. J. Med.* **302**, 589–593 (1980).
7. F. E. Marchlinski, D. J. Callans, C. D. Gottlieb, E. Zado, Linear ablation lesions for control of unmappable ventricular tachycardia in patients with ischemic and nonischemic cardiomyopathy. *Circulation* **101**, 1288–1296 (2000).
8. A. Arenal, E. Glez-Torrecilla, M. Ortiz, J. Villacastín, J. Fdez-Portales, E. Sousa, S. del Castillo, L. Perez de Isla, J. Jimenez, J. Almendral, Ablation of electrograms with an isolated, delayed component as treatment of unmappable monomorphic ventricular tachycardias in patients with structural heart disease. *J. Am. Coll. Cardiol.* **41**, 81–92 (2003).
9. W. G. Stevenson, Catheter ablation of monomorphic ventricular tachycardia. *Curr. Opin. Cardiol.* **20**, 42–47 (2005).
10. V. Y. Reddy, M. R. Reynolds, P. Neuzil, A. W. Richardson, M. Taborsky, K. Jongnarangsin, S. Kralovec, L. Sediva, J. N. Ruskin, M. E. Josephson, Prophylactic catheter ablation for the prevention of defibrillator therapy. *N. Engl. J. Med.* **357**, 2657–2665 (2007).
11. C. Ramanathan, R. N. Ghanem, P. Jia, K. Ryu, Y. Rudy, Noninvasive electrocardiographic imaging for cardiac electrophysiology and arrhythmia. *Nat. Med.* **10**, 422–428 (2004).
12. C. Ramanathan, P. Jia, R. Ghanem, K. Ryu, Y. Rudy, Activation and repolarization of the normal human heart under complete physiological conditions. *Proc. Natl. Acad. Sci. U.S.A.* **103**, 6309–6314 (2006).
13. H. S. Oster, B. Taccardi, R. L. Lux, P. R. Ershler, Y. Rudy, Noninvasive electrocardiographic imaging: Reconstruction of epicardial potentials, electrograms, and isochrones and localization of single and multiple electrocardiac events. *Circulation* **96**, 1012–1024 (1997).
14. J. P. Moak, M. R. Rosen, Induction and termination of triggered activity by pacing in isolated canine Purkinje fibers. *Circulation* **69**, 149–162 (1984).
15. H. S. Oster, B. Taccardi, R. L. Lux, P. R. Ershler, Y. Rudy, Electrocardiographic imaging: Noninvasive characterization of intramural myocardial activation from inverse-reconstructed epicardial potentials and electrograms. *Circulation* **97**, 1496–1507 (1998).
16. J. E. Zimmer, K. Hynynen, D. S. He, F. Marcus, The feasibility of using ultrasound for cardiac ablation. *IEEE Trans. Biomed. Eng.* **42**, 891–897 (1995).
17. S. A. Strickberger, T. Tokano, J. U. A. Kluiwstra, F. Morady, C. Cain, Extracardiac ablation of the canine atrioventricular junction by use of high-intensity focused ultrasound. *Circulation* **100**, 203–208 (1999).
18. A. Sharma, D. Wong, G. Weidlich, T. Fogarty, A. Jack, T. Sumanaweera, P. Maguire, Noninvasive stereotactic radiosurgery (CyberHeart) for creation of ablation lesions in the atrium. *Heart Rhythm* **7**, 802–810 (2010).
19. W. Kaltenbrunner, R. Cardinal, M. Dubuc, M. Shenasa, R. Nadeau, G. Tremblay, M. Vermeulen, P. Savard, P. L. Pagé, Epicardial and endocardial mapping of ventricular tachycardia in patients with myocardial infarction. Is the origin of the tachycardia always subendocardially localized? *Circulation* **84**, 1058–1071 (1991).
20. L. Harris, E. Downar, L. Mickleborough, N. Shaikh, I. Parson, Activation sequence of ventricular tachycardia: Endocardial and epicardial mapping studies in the human ventricle. *J. Am. Coll. Cardiol.* **10**, 1040–1047 (1987).
21. L. Littmann, R. H. Svenson, J. J. Gallagher, J. G. Selle, S. H. Zimmern, J. M. Fedor, P. G. Colavita, Functional role of the epicardium in postinfarction ventricular tachycardia. Observations derived from computerized epicardial activation mapping, entrainment, and epicardial laser photoablation. *Circulation* **83**, 1577–1591 (1991).
22. J. M. de Bakker, M. J. Janse, F. J. Van Capelle, D. Durrer, Endocardial mapping by simultaneous recording of endocardial electrograms during cardiac surgery for ventricular aneurysm. *J. Am. Coll. Cardiol.* **2**, 947–953 (1983).
23. J. E. Burnes, B. Taccardi, Y. Rudy, A noninvasive imaging modality for cardiac arrhythmias. *Circulation* **102**, 2152–2158 (2000).
24. J. E. Burnes, B. Taccardi, R. S. MacLeod, Y. Rudy, Noninvasive ECG imaging of electrophysiologically abnormal substrates in infarcted hearts: A model study. *Circulation* **101**, 533–540 (2000).
25. J. E. Burnes, B. Taccardi, P. R. Ershler, Y. Rudy, Noninvasive electrocardiogram imaging of substrate and intramural ventricular tachycardia in infarcted hearts. *J. Am. Coll. Cardiol.* **38**, 2071–2078 (2001).
26. R. N. Ghanem, J. E. Burnes, A. L. Waldo, Y. Rudy, Imaging dispersion of myocardial repolarization, II: Noninvasive reconstruction of epicardial measures. *Circulation* **104**, 1306–1312 (2001).
27. R. N. Ghanem, P. Jia, C. Ramanathan, K. Ryu, A. Markowitz, Y. Rudy, Noninvasive electrocardiographic imaging (ECGI): Comparison to intraoperative mapping in patients. *Heart Rhythm* **2**, 339–354 (2005).
28. A. Intini, R. N. Goldstein, P. Jia, C. Ramanathan, K. Ryu, B. Giannattasio, R. Gilkeson, B. S. Stambler, P. Brugada, W. G. Stevenson, Y. Rudy, A. L. Waldo, Electrocardiographic imaging (ECGI), a novel diagnostic modality used for mapping of focal left ventricular tachycardia in a young athlete. *Heart Rhythm* **2**, 1250–1252 (2005).
29. P. Jia, C. Ramanathan, R. N. Ghanem, K. Ryu, N. Varma, Y. Rudy, Electrocardiographic imaging of cardiac resynchronization therapy in heart failure: Observation of variable electrophysiologic responses. *Heart Rhythm* **3**, 296–310 (2006).
30. Y. Wang, P. S. Cuculich, P. K. Woodard, B. D. Lindsay, Y. Rudy, Focal atrial tachycardia after pulmonary vein isolation: Noninvasive mapping with electrocardiographic imaging (ECGI). *Heart Rhythm* **4**, 1081–1084 (2007).
31. Y. Wang, R. B. Schuessler, R. J. Damiano, P. K. Woodard, Y. Rudy, Noninvasive electrocardiographic imaging (ECGI) of scar-related atypical atrial flutter. *Heart Rhythm* **4**, 1565–1567 (2007).
32. Y. Wang, L. Li, P. S. Cuculich, Y. Rudy, Electrocardiographic imaging of ventricular bigeminy in a human subject. *Circ. Arrhythm. Electrophysiol.* **1**, 74–75 (2008).
33. S. Ghosh, E. K. Rhee, J. N. Avari, P. K. Woodard, Y. Rudy, Cardiac memory in patients with Wolff-Parkinson-White syndrome: Noninvasive imaging of activation and repolarization before and after catheter ablation. *Circulation* **118**, 907–915 (2008).
34. S. Ghosh, J. N. Avari, E. K. Rhee, P. K. Woodard, Y. Rudy, Noninvasive electrocardiographic imaging (ECGI) of epicardial activation before and after catheter ablation of the accessory pathway in a patient with Ebstein anomaly. *Heart Rhythm* **5**, 857–860 (2008).
35. S. Ghosh, J. N. Avari, E. K. Rhee, P. K. Woodard, Y. Rudy, Hypertrophic cardiomyopathy with preexcitation: Insights from noninvasive electrocardiographic imaging (ECGI) and catheter mapping. *J. Cardiovasc. Electrophysiol.* **19**, 1215–1217 (2008).
36. S. Ghosh, J. N. Avari, E. K. Rhee, P. K. Woodard, Y. Rudy, Noninvasive electrocardiographic imaging (ECGI) of a univentricular heart with Wolff-Parkinson-White syndrome. *Heart Rhythm* **5**, 605–608 (2008).
37. Y. Wang, Y. Rudy, Electrocardiographic imaging of normal human atrial repolarization. *Heart Rhythm* **6**, 582–583 (2009).
38. J. N. Silva, S. Ghosh, T. M. Bowman, E. K. Rhee, P. K. Woodard, Y. Rudy, Cardiac resynchronization therapy in pediatric congenital heart disease: Insights from noninvasive electrocardiographic imaging. *Heart Rhythm* **6**, 1178–1185 (2009).
39. N. Varma, P. Jia, C. Ramanathan, Y. Rudy, RV electrical activation in heart failure during right, left, and biventricular pacing. *JACC Cardiovasc. Imaging* **3**, 567–575 (2010).
40. P. S. Cuculich, Y. Wang, B. D. Lindsay, R. Vijayakumar, Y. Rudy, Noninvasive real-time mapping of an incomplete pulmonary vein isolation using electrocardiographic imaging. *Heart Rhythm* **7**, 1316–1317 (2010).
41. P. S. Cuculich, Y. Wang, B. D. Lindsay, M. N. Faddis, R. B. Schuessler, R. J. Damiano Jr., L. Li, Y. Rudy, Noninvasive characterization of epicardial activation in humans with diverse atrial fibrillation patterns. *Circulation* **122**, 1364–1372 (2010).
42. S. Ghosh, D. H. Cooper, R. Vijayakumar, J. Zhang, S. Pollack, M. Haissaguerre, Y. Rudy, Early repolarization associated with sudden death: Insights from noninvasive electrocardiographic imaging. *Heart Rhythm* **7**, 534–537 (2010).
43. F. Ouyang, P. Fotuhi, S. Y. Ho, J. Hebe, M. Volkmer, M. Goya, M. Burns, M. Antz, S. Ernst, R. Cappato, K. H. Kuck, Repetitive monomorphic ventricular tachycardia originating from the aortic sinus cusp: Electrocardiographic characterization for guiding catheter ablation. *J. Am. Coll. Cardiol.* **39**, 500–508 (2002).

44. D. Lin, L. Ilkhanoff, E. Gerstenfeld, S. Dixit, S. Beldner, R. Bala, F. Garcia, D. Callans, F. E. Marchlinski, Twelve-lead electrocardiographic characteristics of the aortic cusp region guided by intracardiac echocardiography and electroanatomic mapping. *Heart Rhythm* **5**, 663–669 (2008).

45. **Acknowledgments:** We thank T. Street and S. Ghosh for their help in this study. **Funding:** This study was supported by NIH–National Heart, Lung, and Blood Institute grants R01-HL-033343-26 and R01-HL-049054-18 (to Y.R.) and grants 1 UL1 RR024992-01, 1 TL1 RR024995-01, and 1 KL2 RR 024994-01 from the National Center for Research Resources of the NIH. Y.R. is the Fred Saigh Distinguished Professor at Washington University in St. Louis. **Author contributions:** Y.W., P.S.C., and Y.R. devised the experiments. Y.W., P.S.C., J.Z., K.A.D., R.V., J.C., M.N.F., B.D.L., and T.W.S. performed the experiments. Y.W., P.S.C., J.Z., K.A.D., R.V., and Y.R. performed data analysis. Y.W., P.S.C., and Y.R. wrote the manuscript. All authors reviewed and edited the manuscript. Y.R. provided funding. **Competing interests:** Y.R. co-chairs the scientific advisory board of and holds equity in CardioInsight Technologies. CardioInsight Technologies does not support any research conducted by Y.R., including that presented here. B.D.L. is a member of the scientific advisory board of CardioInsight Technologies. The following patents are related to ECGI technology and owned by the university where the research was conducted: U.S. patent number 6772004, "System and Method for Non-invasive Electrocardiographic Imaging," Case Western Reserve University; U.S. patent number 6975900, "Systems and Methods for Determining Surface Geometry," Case Western Reserve University; U.S. patent number 7016719 "System and Method for Non-invasive Electrocardiographic Imaging (ECGI) Using Generalized Minimum Residual (GMRes)," Case Western Reserve University; U.S. patent number 7471973, "Determining a Surface Geometry of an Object," Case Western Reserve University; "System and Methods for On-site and Real Time Electrocardiographic Imaging (ECGI)," submitted to Washington University; "A Fast, Mesh-Free Numerical Method for Noninvasive Electrocardiographic Imaging," submitted to Washington University.

Submitted 18 January 2011
Accepted 23 June 2011
Published 31 August 2011
10.1126/scitranslmed.3002152

Citation: Y. Wang, P. S. Cuculich, J. Zhang, K. A. Desouza, R. Vijayakumar, J. Chen, M. N. Faddis, B. D. Lindsay, T. W. Smith, Y. Rudy, Noninvasive electroanatomic mapping of human ventricular arrhythmias with electrocardiographic imaging (ECGI). *Sci. Transl. Med.* **3**, 98ra84 (2011).